Journal of Computer Assisted Tomography
13(5):779–788, September/October

Rapid Three-dimensional Display of the Cerebral Ventricles from Noncontrast CT Scans

Thomas P. Naidich, Bruce C. Teeter, Arthur Nieves, Carl R. Crawford, Erin Prenger, and David G. McLone

Abstract: Three-dimensional images of the cerebral ventricles may now be generated from routine serial axial or coronal noncontrast CT scans in 5–8 min and rotated in space interactively in 2–5 s to provide the physician with useful views of anatomic relationships difficult to depict in other ways. **Index Terms:** Brain, anatomy—Children—Cerebrospinal fluid—Computed tomography—Hydrocephalus—Computed tomography, three-dimensional—Brain, ventricles.

Previous authors have successfully displayed three-dimensional (3D) CT images of the cerebral ventricles (1–9). As a rule, however, these have required intraventricular instillation of positive contrast agent; have needed long processing times requiring the images to be constructed off line, usually overnight; and have provided limited numbers of views (1,4,6). This paper presents our experience with rapid generation of 3D CT images of the cerebral ventricles from standard noncontrast axial or coronal CT scans of the head. The images may be generated, manipulated interactively, and filmed onto hard copy in a total time of approximately 10–12 min. This is sufficiently rapid that the entire procedure may be performed between patients, during room cleaning and preparation, with no significant reduction in patient throughput. To our knowledge, no prior communication has discussed interactive, 3D CT display of the cerebral ventricles, nor has any demonstrated the 3D CT appearance of the ventricles in such a broad range of pathology.

MATERIALS AND METHODS

The study material consisted of 3D images generated from routine noncontrast axial or coronal CT scans from 64 pediatric patients: 34 girls and 30 boys, 1 day to 18.5 years old (mean age 3.35 years). Of these 64 patients, 8 (13%) had infratentorial tumors, 7 (11%) had supratentorial tumors, 12 (19%) had hydrocephalus of diverse etiologies, and 36 (56%) had congenital malformations (schizencephaly 10, callosal agenesis 8, Dandy Walker malformation or variant 7, arachnoid cyst 5, Chiari II malformation 2, holoprosencephaly 2, hydranencephaly 1, and migrational disorder 1).

In practice, standard axial or coronal CT scans were obtained on a GE CT/T 9800 Quick scanner utilizing 120 kV, 20–35 mA (low-dose dynamic mode), 2 s scan time, and variable, often mixed, slice thicknesses of 1.5 mm, 3 mm, or 5 mm. To reduce patient motion and improve the 3D images, it proved useful to obtain the initial series of CT slices as dynamic scans. Three-dimensional surfaces of the ventricles were then generated by the method of dividing cubes (9) using the standard operator's console, the Quick-3D option on the GE CT/T 9800 scanner, and standard image data.

No contrast agent was used to opacify the CSF. Instead, the system was instructed to recognize only those pixels with specific CT numbers, typically 4–7 units inclusive, to create a surface that corresponded to CSF only (Fig. 1). The precise range of numbers was somewhat individual and case dependent, occasionally requiring some trial and error for optimum results. The surface that was generated faithfully reproduced the contour of the ventricles (Fig. 2).

The surface was rotated in space, as desired, by instructing the computer to rotate the image around the three mutually orthogonal axes, *X*, *Y*, or *Z*, any

From the Baptist Hospital of Miami, Department of Radiology, Miami, FL (T. P. Naidich); General Electric Medical Systems, Milwaukee, WI (B. C. Teeter, A. Nieves, and C. R. Crawford); Barrow Neurological Institute, Phoenix, AZ (E. Prenger); and Division of Neurosurgery, Children's Memorial Hospital, Chicago, IL (D. G. McLone). Address correspondence and reprint requests to Dr. T. P. Naidich at Department of Radiology, Baptist Hospital of Miami, 8900 North Kendall Drive, Miami, FL 33176–2197.

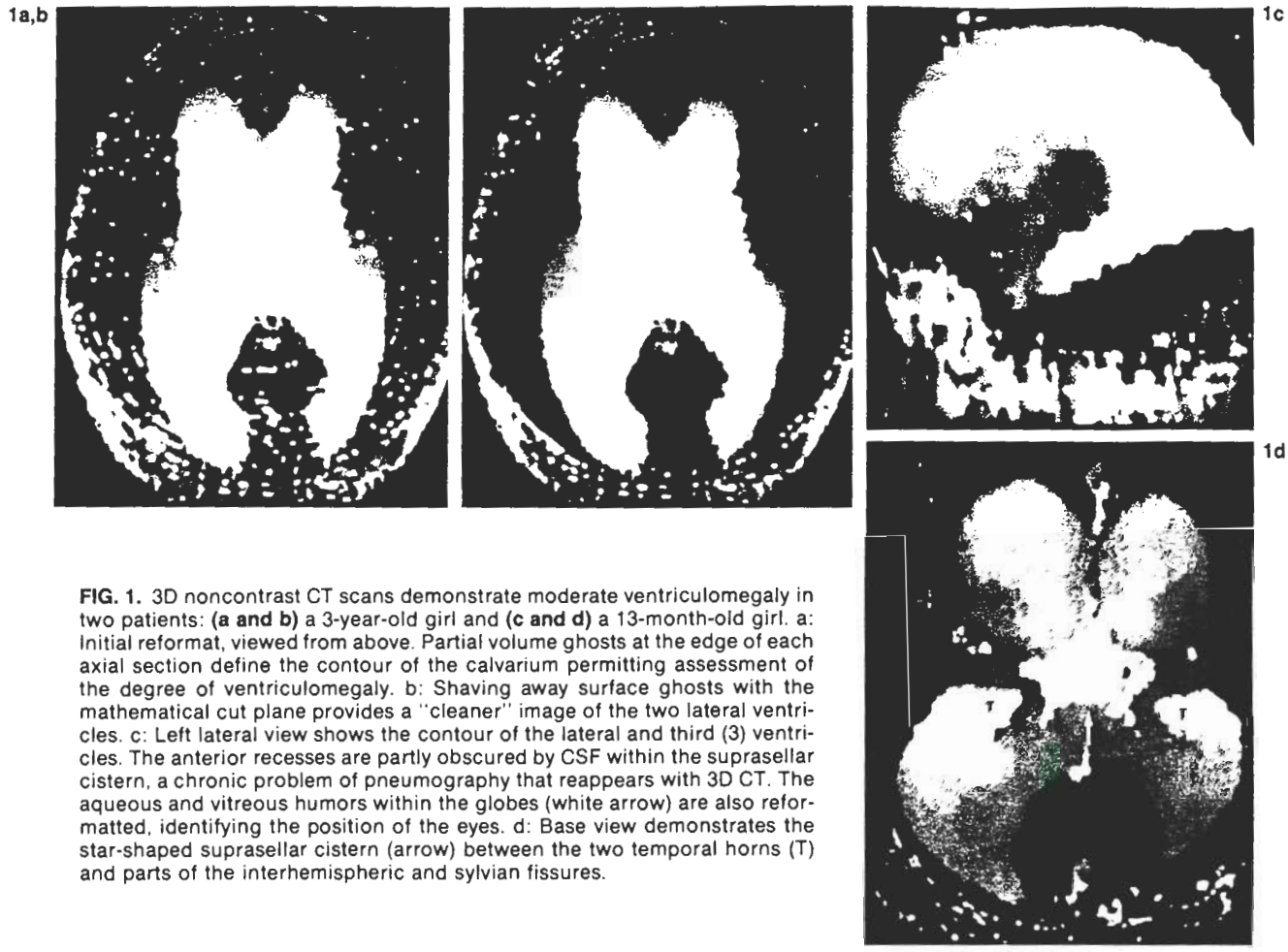

FIG. 1. 3D noncontrast CT scans demonstrate moderate ventriculomegaly in two patients: **(a and b)** a 3-year-old girl and **(c and d)** a 13-month-old girl. a: Initial reformat, viewed from above. Partial volume ghosts at the edge of each axial section define the contour of the calvarium permitting assessment of the degree of ventriculomegaly. b: Shaving away surface ghosts with the mathematical cut plane provides a "cleaner" image of the two lateral ventricles. c: Left lateral view shows the contour of the lateral and third (3) ventricles. The anterior recesses are partly obscured by CSF within the suprasellar cistern, a chronic problem of pneumography that reappears with 3D CT. The aqueous and vitreous humors within the globes (white arrow) are also reformatted, identifying the position of the eyes. d: Base view demonstrates the star-shaped suprasellar cistern (arrow) between the two temporal horns (T) and parts of the interhemispheric and sylvian fissures.

specific number of degrees, e.g., counterclockwise 37° (Fig. 3). The surfaces were also "sliced" by moving them into or out of a mathematical cut plane to remove unwanted structures or to expose specific portions of anatomy (Fig. 1b). The system could also be instructed to generate a surface that corresponded to all pixels within a wider range of numbers, typically −80 to +7 units inclusive. This

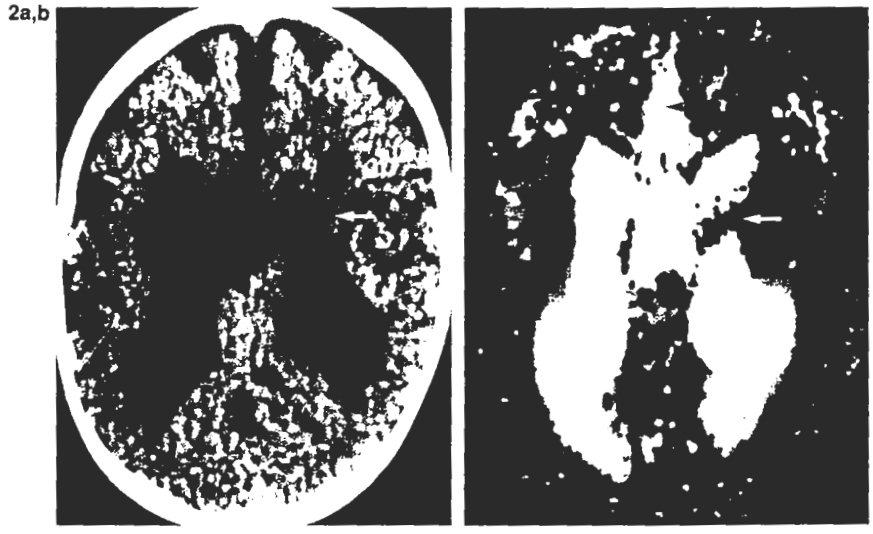

FIG. 2. Callosal agenesis in a 6-month-old boy. **a:** Axial noncontrast CT scan demonstrates callosal agenesis with enlarged, separated lateral ventricles, deformity (white arrow) of the medial wall of the left lateral ventricle, wide interhemispheric fissure containing the falx, and enlarged sulci. **b:** Reformatted 3D, noncontrast CT scan faithfully reproduces the contour of the lateral ventricles, the defect (white arrow) in the body of the left lateral ventricle, and the position of the falx (black arrowhead) within the widened interhemispheric fissure. The widened sulci are reproduced but are less conspicuous on the 3D image because they merge with the ghosts.

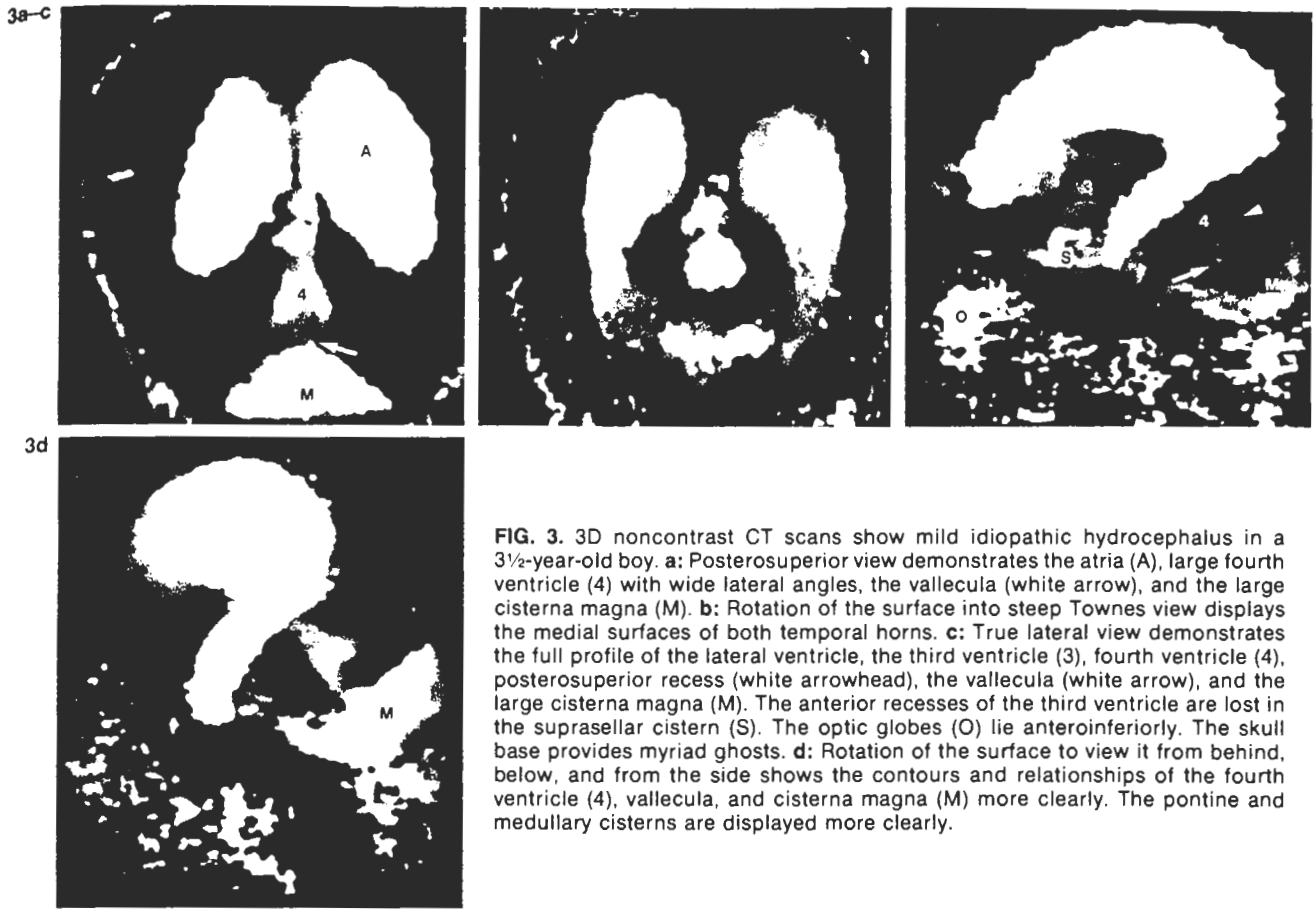

FIG. 3. 3D noncontrast CT scans show mild idiopathic hydrocephalus in a 3½-year-old boy. **a:** Posterosuperior view demonstrates the atria (A), large fourth ventricle (4) with wide lateral angles, the vallecula (white arrow), and the large cisterna magna (M). **b:** Rotation of the surface into steep Townes view displays the medial surfaces of both temporal horns. **c:** True lateral view demonstrates the full profile of the lateral ventricle, the third ventricle (3), fourth ventricle (4), posterosuperior recess (white arrowhead), the vallecula (white arrow), and the large cisterna magna (M). The anterior recesses of the third ventricle are lost in the suprasellar cistern (S). The optic globes (O) lie anteroinferiorly. The skull base provides myriad ghosts. **d:** Rotation of the surface to view it from behind, below, and from the side shows the contours and relationships of the fourth ventricle (4), vallecula, and cisterna magna (M) more clearly. The pontine and medullary cisterns are displayed more clearly.

technique created dual surfaces that displayed "skin" and CSF simultaneously (Fig. 4). As with the CSF surface, the optimal window width and level varied slightly from case to case.

The image appearance was substantially improved by increasing ambient lighting and depth shading to nearly maximum. Early experience taught that artifacts arising from the Velcro restraint interfered with the construction of a smooth, anatomic skin surface (Fig. 4b and c). Restraint by Micropore tape (3M, St. Paul, MN, U.S.A.) proved a satisfactory solution to this problem.

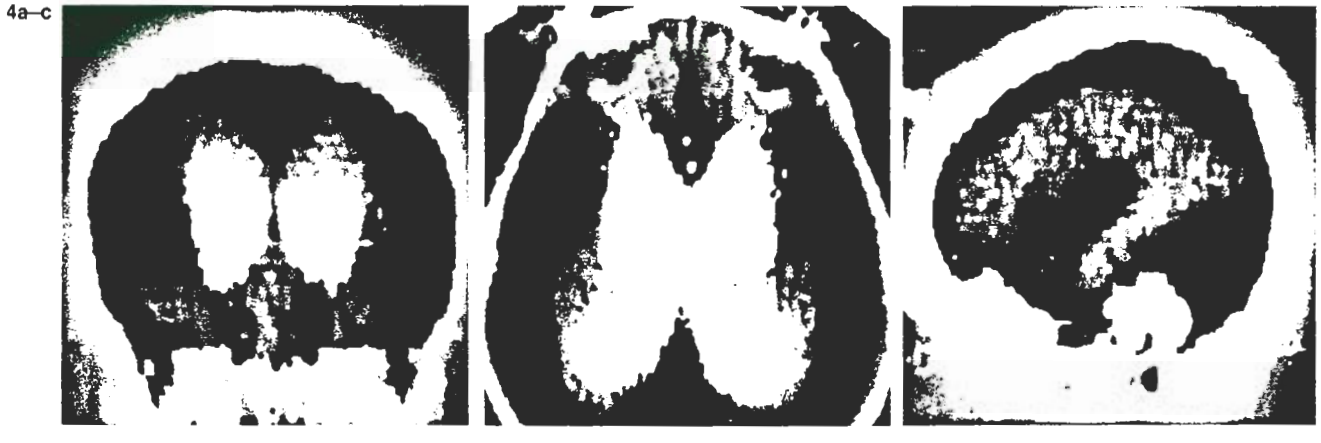

FIG. 4. 3D noncontrast CT scans demonstrate dual skin-CSF surfaces in a 22-month-old boy with mild hydrocephalus. **a:** Anterior view. **b:** Superior view. **c:** Lateral view. Portions of the skin have been shaved away to provide windows for viewing the ventricles. Simultaneous display of the skin surface and the ventricles provides valuable landmarks for selecting the entry point for placing shunt catheters.

5a,b

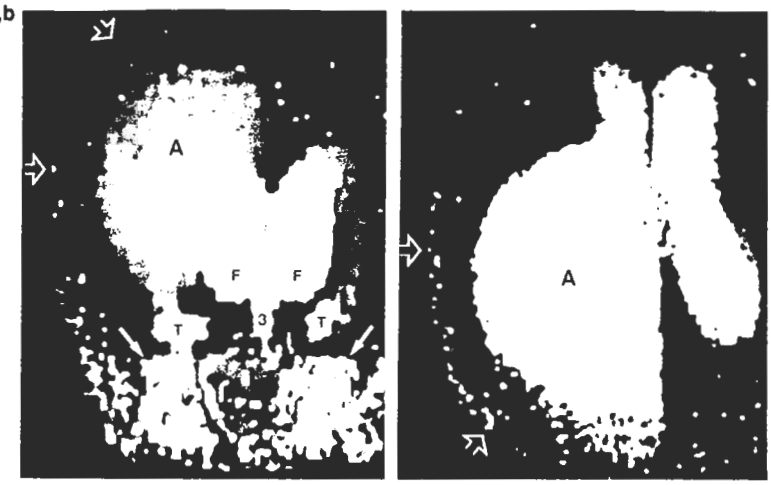

FIG. 5. 3D noncontrast CT scans show asymmetric atrial dilatation with calvarial expansion in a 23-month-old boy. Frontal **(a)** and superior **(b)** views document that the asymmetric expansion (open arrows) of the hemicalvarium results from relatively focal ballooning of the atrium (A) with little, if any, midline shift. Frontal horns (F), temporal horns (T), and third ventricle (3) are slightly dilated. The globes (solid arrows) appear in proper position in the images.

Image quality was graded subjectively, by the consensus of two observers, as excellent, good, fair, or poor.

RESULTS

The 3D images of the ventricles could be generated easily from either axial or coronal CT slices. In general, axial slices proved superior, because coronal images of the posterior portion of the head passed through the thorax, introducing artifact from respiratory motion. The time to generate the 3D surface depended primarily on the number of slices obtained. Less important variables in determining the time needed to generate the surface were the size of the ventricles and the height of the specific threshold chosen (or the width of the range of numbers chosen). In the typical case, image reformatting from 30 slices required 5 min; 3D reformatting from 80 slices required 8 min. Once the 3D surface was generated, that surface would be rotated, obliqued, and sliced to obtain a specific view of the surface in 2–5 s per manipulation, depending on what else the system was doing at the time.

Experience quickly standardized the 3D series into seven major images: anterior, posterior, left, right, top, and bottom views of the entire ventricular system plus a nearly midline slice for the third ventricle. In practice, it proved advantageous to view the full thickness of the third ventricle from slightly off midline rather than from the midline itself. Additional images were obtained ad lib to emphasize whatever features of the case seemed most relevant. Oblique views with both canting and rotation frequently enhanced the sense of depth and the 3D effect, so posterosuperolateral and anteroinferolateral views were often added to the routine series. Each 3D image selected was stored on the disk for transfer to the tape archives by using the "screen save" feature.

Because the 3D surfaces are generated from image data and stored on disk or in tape archives, any error in choosing the proper obliquity, and any errors in filming the surfaces could be corrected sim-

6a,b

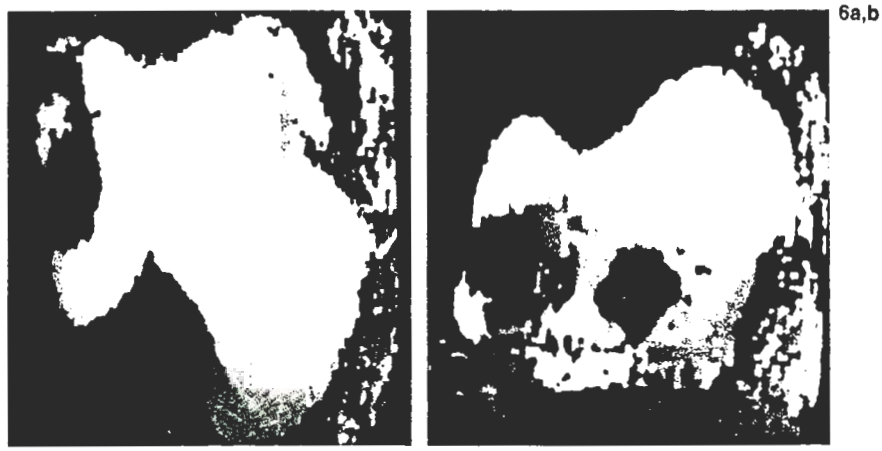

FIG. 6. 3D noncontrast CT scans demonstrate left hemiatrophy in a 13-year-old boy. **a:** Superior view. **b:** Posterior view. Unilateral ventricular dilatation, ipsilateral expansion of the convexity subarachnoid spaces, and tilting of the midline toward the expanded ventricle indicate juvenile hemiatrophy.

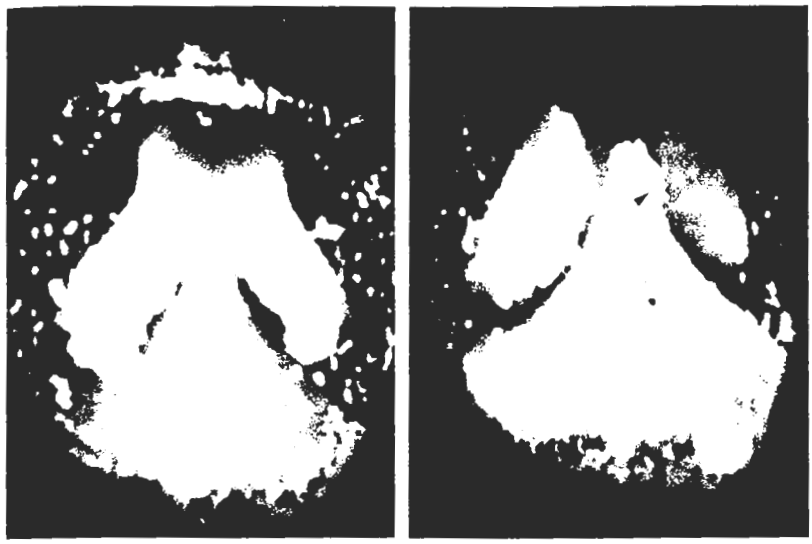

FIG. 7. 3D noncontrast CT scans show Dandy-Walker malformation in a 1-day-old girl. Superior **(a)** and posterosuperior oblique **(b)** views demonstrate the relationship of the fourth ventricular cyst to the splayed atria and to the inferior surface of the falx that notches (arrowhead, b) the top of the cyst.

ply by re-creating the surface for viewing by the physician. Since raw data are not required, 3D CT images can be generated at will from any old tape in the archives. There is no need to determine in advance whether 3D reformating will be required for any particular patient; it can be generated from the tape archive, whenever desired.

Three-dimensional CT easily displayed dilatation of specific ventricular chambers and large subarachnoid cisterns, so unilateral atrial dilatation (Fig. 5) could be easily distinguished from hemiatrophy (Fig. 6). Three-dimensional CT clearly depicted the characteristic ventricular anomalies of Dandy-Walker malformations (Fig. 7), holoprosencephaly (Fig. 8), open-lip schizencephaly (Fig. 9), and callosal agenesis (Fig. 10). Three-dimensional CT demonstrated severe periventricular edema as irregularity of the ventricular margin (Fig. 11a) and low-density tumor as a patchy mass (Fig. 11b). Three-dimensional CT was particularly useful for demonstrating the relationships of posterior fossa tumors to the fourth ventricle and aqueduct (Fig. 11c and d) and of supratentorial tumors to the lateral and third ventricles (Figs. 12 and 13).

The images generated were judged to be excellent in 28 cases (44%), good in 20 cases (31%), fair in 9 cases (14%), and poor in 7 cases (11%). Poor quality was usually the result of patient motion during the initial CT series. However, poor 3D images were also frequent in patients with extremely large ventricles, because so little parenchyma remained to separate and to give definition to the individual chambers.

Partial volume phenomena were a major cause of troublesome artifacts or "ghosts" in many of the images. At the interfaces between air and soft tis-

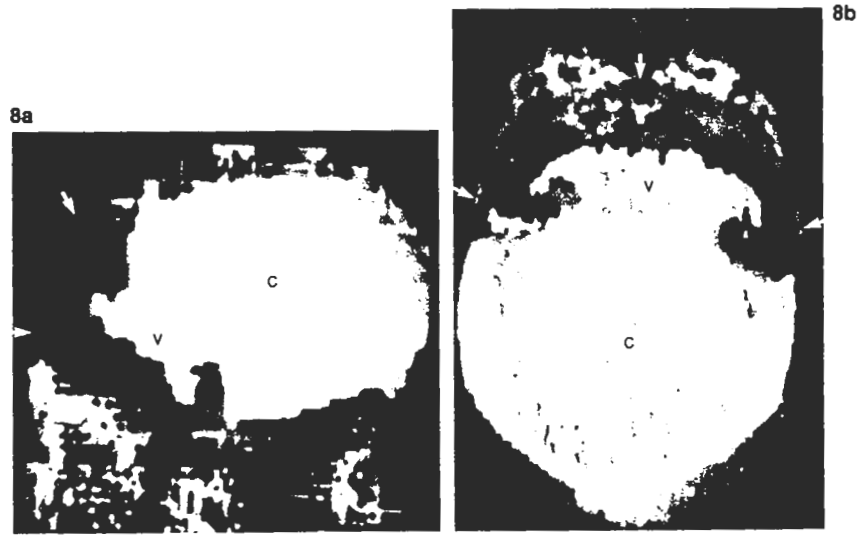

FIG. 8. 3D noncontrast CT scans show holoprosencephaly with dorsal cyst in a 1-day-old girl. In each image floaters and a small portion of the ventricle have been shaved away. **a:** Lateral view demonstrates the monoventricle (V) and the dorsal cyst (C). The shape of the holoprosencephalon (white arrows) must be inferred from the contour of the ventricles and the ghosts. **b:** Axial view with the superior portion of the ventricle shaved away confirms the contour of the monoventricle (V), dorsal cyst (C), and holoprosencephalon (white arrows) in a familiar plane.

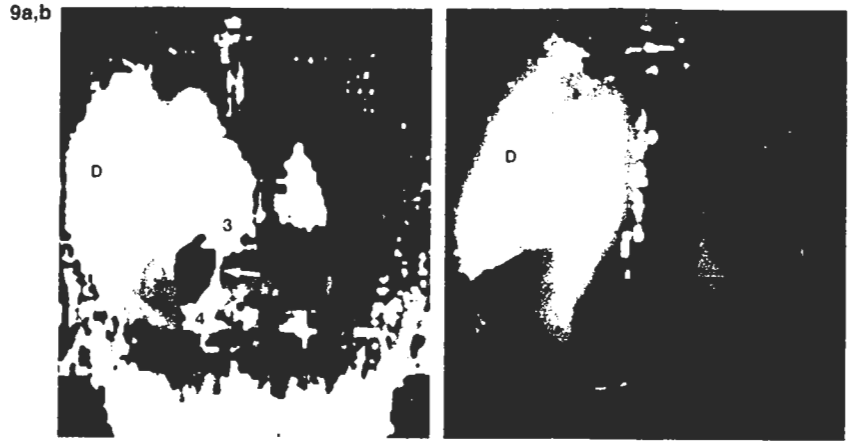

FIG. 9. 3D noncontrast CT scans show unilateral open-lip schizencephaly in a 7-month-old girl. Posterior **(a)** and superior **(b)** views demonstrate right hemiatrophy with smaller right hemicalvarium and a larger right lateral ventricle that communicates broadly with a wide fan-shaped diverticulum (D) in the general region of the island of Reil and the sylvian fissure. The interhemispheric fissure is widened on each side of the falx. The posterior third ventricle (3), aqueduct (white arrow), and fourth ventricle (4) are also seen in (a).

sue, between air and bone, and between fat and bone, the partial volume effect created pixels with the same CT number as CSF. These pixels appeared as "floaters," separate from the main body of CSF (Fig. 1). The finite resolution of the system, limited by the finite area of the focal spots and detectors and by the reconstruction kernels, also generated floaters.

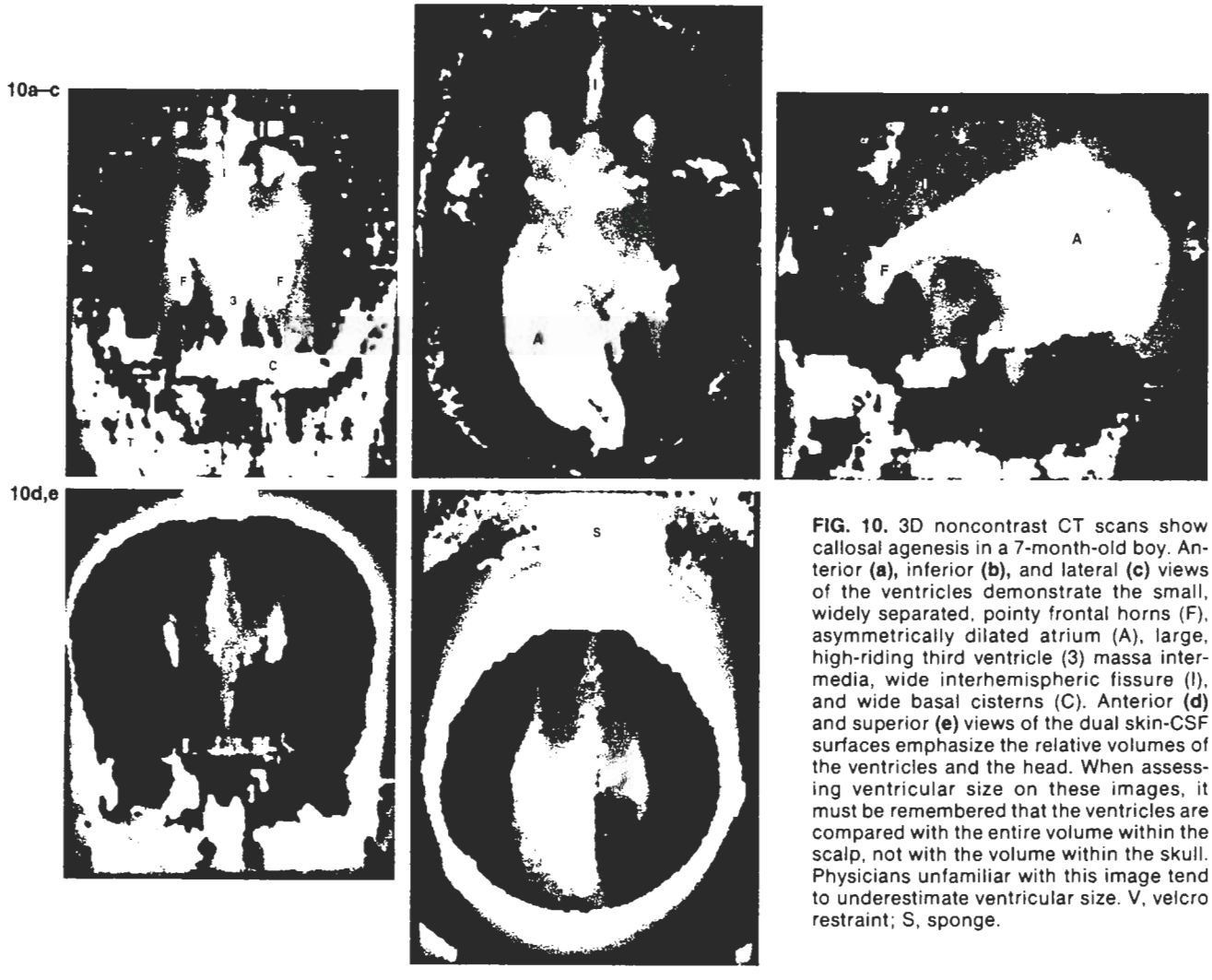

FIG. 10. 3D noncontrast CT scans show callosal agenesis in a 7-month-old boy. Anterior **(a),** inferior **(b),** and lateral **(c)** views of the ventricles demonstrate the small, widely separated, pointy frontal horns (F), asymmetrically dilated atrium (A), large, high-riding third ventricle (3) massa intermedia, wide interhemispheric fissure (I), and wide basal cisterns (C). Anterior **(d)** and superior **(e)** views of the dual skin-CSF surfaces emphasize the relative volumes of the ventricles and the head. When assessing ventricular size on these images, it must be remembered that the ventricles are compared with the entire volume within the scalp, not with the volume within the skull. Physicians unfamiliar with this image tend to underestimate ventricular size. V, velcro restraint; S, sponge.

The floaters partially obscure the ventricular surface, but experienced radiologists can easily read through them to assess size and configuration of the ventricles. The floaters do become intermixed with true CSF pixels of the subarachnoid space, making interpretation of extracerebral CSF spaces difficult. The number of floaters can be reduced by using the shave plane to shear them away (Fig. 1b). In the laboratory they can be removed by using a custom-designed, region-growing algorithm tailored to the ventricles to segment the ventricles from the rest of the image. In the hospital the floaters can be eliminated most easily by incorporating them into the skin surface of a wide threshold (approximately −80 to +7) skin/CSF image (Fig. 4). In practice, it proved preferable to leave the floaters intact, because they outlined the size and shape of the skull and thereby provided a scale against which to judge the degree of ventriculomegaly (Figs. 1 and 3).

When CT reformatting used the wide threshold of −80 to +7 units, air–bone and fat–bone interfaces may also outline the roofs of the orbits and the paranasal sinuses (Fig. 4). These provide additional landmarks for assessing the relationship of the ventricles to their bony and soft tissue envelopes.

DISCUSSION

The 3D effect and the overall image brightness are determined by three "lighting" effects: diffuse reflection, depth queuing (shading), and ambient lighting. The brightness observed at any point on an

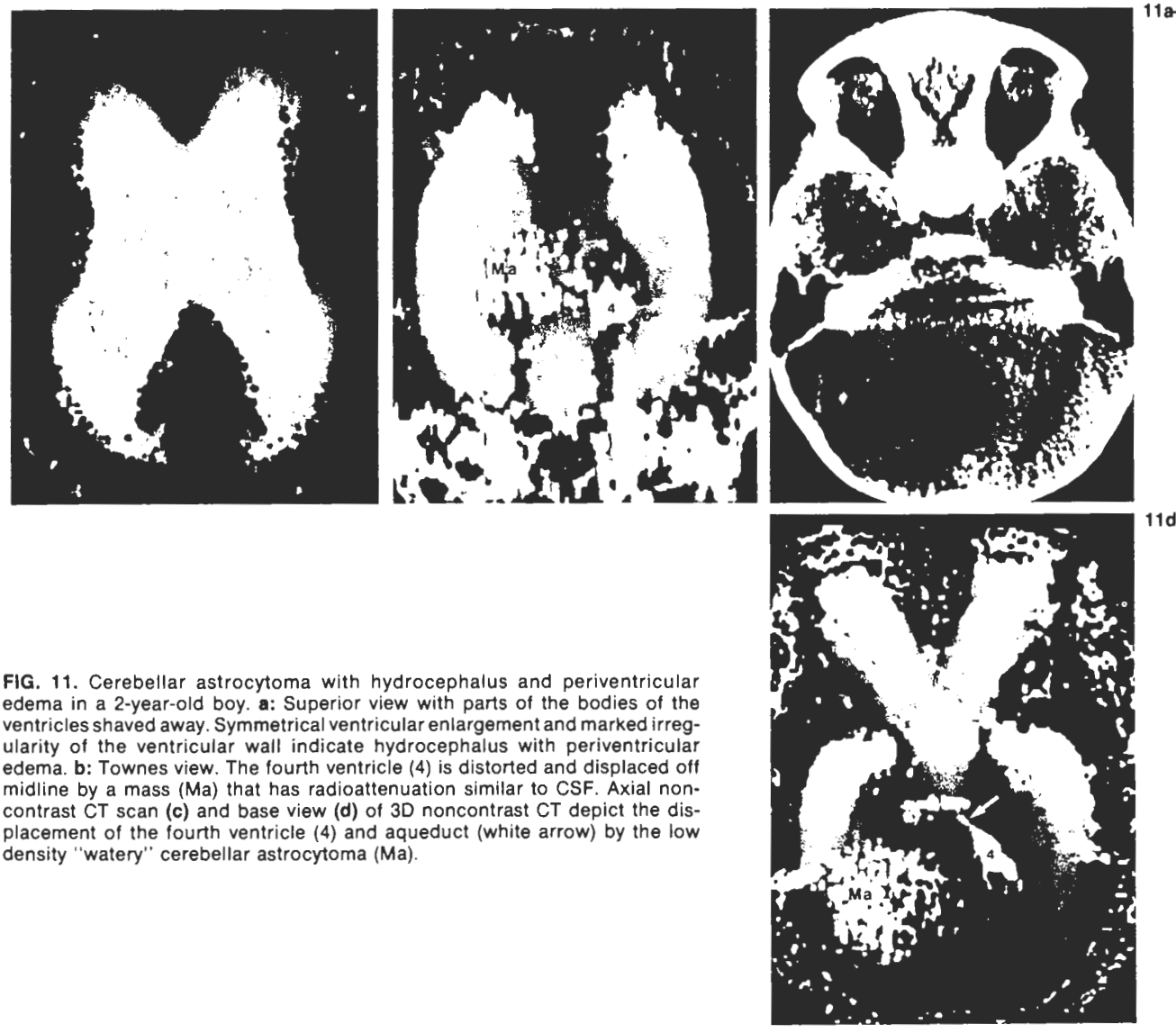

FIG. 11. Cerebellar astrocytoma with hydrocephalus and periventricular edema in a 2-year-old boy. **a:** Superior view with parts of the bodies of the ventricles shaved away. Symmetrical ventricular enlargement and marked irregularity of the ventricular wall indicate hydrocephalus with periventricular edema. **b:** Townes view. The fourth ventricle (4) is distorted and displaced off midline by a mass (Ma) that has radioattenuation similar to CSF. Axial noncontrast CT scan **(c)** and base view **(d)** of 3D noncontrast CT depict the displacement of the fourth ventricle (4) and aqueduct (white arrow) by the low density "watery" cerebellar astrocytoma (Ma).

12a,b

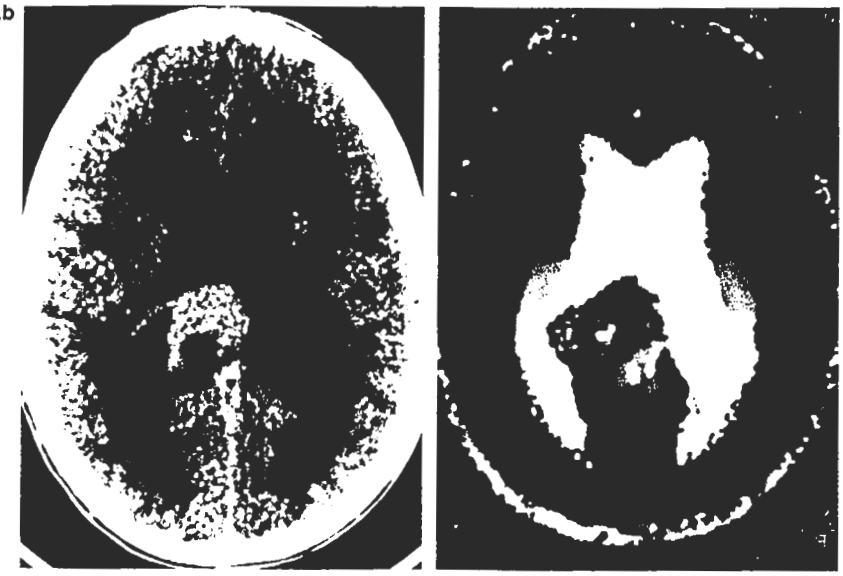

FIG. 12. Extraventricular thalamic astrocytoma in a 7½-year-old boy. **a:** Intravenously enhanced axial CT scan. **b:** Superior view of 3D CT. The exophytic thalamic mass compresses the inferomedial portion of the atrium and deforms the cistern of the vein of Galen.

image depends on the relative weighting that the computer gives to each of these three factors. In *diffuse reflection* one assumes that there is a single source of light that shines on each square unit of the image surface. Depending on the angle which that square unit makes with the source, a variable amount of light will be reflected back to the viewer. This effect gives the shape of the object. The accuracy of the shape will depend on how precisely one can determine the angle between the source and the specific square unit of surface. In *depth queuing* (shading) the computer attenuates the brightness of each square unit as a function of how far that unit lies from the light source. Squares situated farther from the source appear darker. In *ambient lighting* one assumes that all square units reflect equally and adjusts the total reflections to achieve an overall image brightness that is independent of either shape or depth.

In 3D reformatting of bone there usually is high contrast between the bone-containing pixels and the surrounding soft tissue. The position and angle of each square unit can be determined relatively precisely. Therefore, 3D surface reformatting of bone gives heavy weighting to diffuse reflection and adds a moderate amount of depth shading. Ambient lighting is held to a minimum.

In 3D reformatting of the ventricles there is inherently poorer contrast between the CSF and the surrounding brain. There is greater noise, so the

13a,b

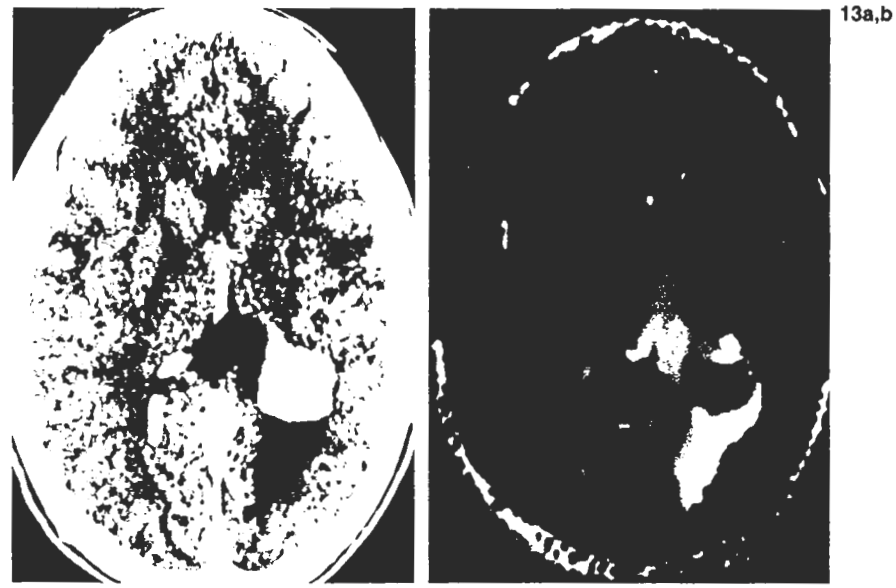

FIG. 13. Intraventricular choroid plexus papilloma in a 6-year-old girl. **a:** Intravenously enhanced axial CT scan shows the densely enhancing intraventricular mass arising from the glomus of the choroid plexus. **b:** 3D CT scan displays the filling defect of the mass within the distended atrium.

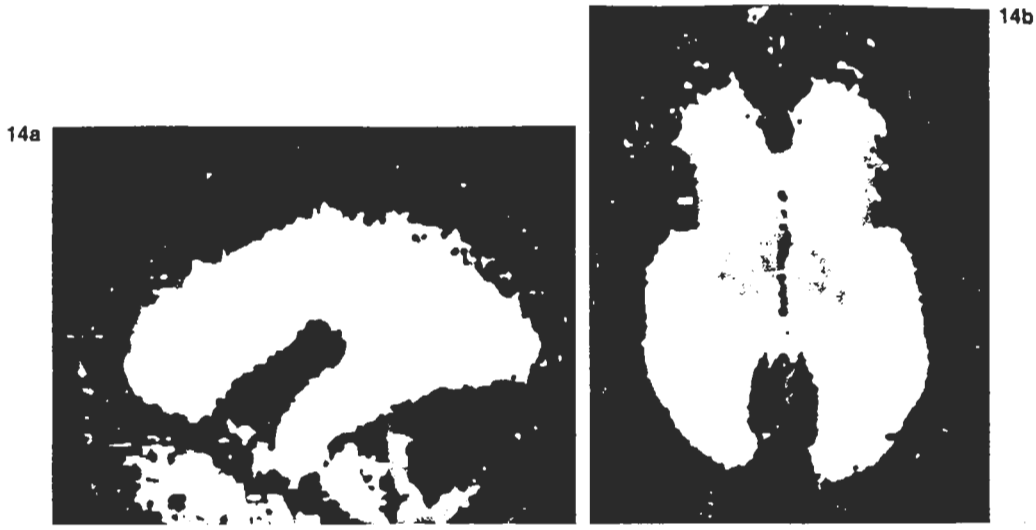

FIG. 14. 3D noncontrast CT scans show hypothalamic glioma in a 22-month-old boy. Lateral **(a)** and base **(b)** views demonstrate a filling defect that nearly obliterates the third ventricle and the suprasellar cistern (compare with Fig. 1c and d). The pontine and medullary cisterns are widened. The fourth ventricle is displaced posteriorly. Ventricular enlargement and prominent irregularity of the ventricular walls indicate obstructive hydrocephalus with periventricular edema.

position and angle of each square unit of surface cannot be determined precisely. The estimate of diffuse reflection is corrupt. Therefore, diffuse reflection is given a low weighting. Depth shading is increased to near maximum, and the overall image brightness is improved by increasing the ambient lighting tremendously. As a consequence, the computerized image resembles an actual photograph less closely. However, the degradation does not interfere significantly with medical evaluation of the gross features of the ventricles for which the images are used (Fig. 14).

The 3D surfaces of the ventricles have proved useful in daily practice. Neurosurgeons have judged them to be helpful for appreciating the true size and configuration of the ventricles prior to shunting and for conceptualizing the extent of ventricular decompression following shunting. Although all agree that the same information is available on the serial axial images, many physicians find it easier to appreciate that information from two or three views of the 3D surface reformatting, than from mental integration of multiple serial planar images. Clinician requests for surface reformatting of the ventricles have increased steadily since their introduction.

Surgeons have found that combined skin/CSF dual surface reformatting is useful to them for planning where to place a shunt tube. Display of a focal coarctation in one lateral ventricle influences choice of which side to shunt. Display of the ventricular contour with respect to a specific external landmark aids in determining where to make the skin incision and where to place the burr hole for entry into the atrium of the ventricle (Fig. 4).

Three-dimensional images also help in precise identification of each part of the ventricle, such as in distinguishing frontal horn from anterior body. On serial axial images the portion of the lateral ventricle that lies farthest anteriorly changes imperceptibly from cut to cut. Inferiorly, it is the frontal horn. More superiorly, it is the anterior part of the body. No landmark differentiates these portions. In patients with juxtaventricular pathology it may be very difficult to discern precisely which part of the ventricular system is affected without using 3D CT. In congenital malformations such as schizencephaly, precise analysis of the relationship of the ventricular diverticula to the frontal horn and/or body of the ventricle is extremely difficult in serial axial images but simple in 3D CT (Fig. 9). Similarly, surgeons have found that 3D-surface reformatting helps them understand the volumetric relationships of tumors to the ventricle, facilitating their surgical planning and the confidence with which they attack the deep (ventricular) surface of the tumors.

CONCLUSION

Three-dimensional noncontrast CT accomplishes, in safety and comfort, nearly all the goals of isocentric rotation full volume replacement pneumoventriculography. Only the question of (free) communication of the CSF space(s) remains unresolved. Although all the information shown by 3D surface reformatting is already available from serial planar images, important parts of that information are much easier to appreciate from 3D images than from serial planar cuts. The fuller appreciation of that information aids the surgeon to plan therapy

and to assess the results of therapy. In the authors' opinion, that difference is a sufficient basis for using 3D surface reformatting of the ventricles in selected cases.

Acknowledgment: The authors thank Mike Tangorra, Children's Memorial Hospital, for picture production; Sidney Dent, Sandy Huebner, Patty Garland, Rebecca Sheesley, Olga Kweicien, Mike Angellini, and, very especially, Augustus Lewis, for producing the 3D images; and Gloria Short, for organization, and Susan DeBusk, for manuscript production.

REFERENCES

1. Batnitzky S, Price HI, Cook PN, Cook LT, Dwyer SJ III. Three-dimensional computer reconstruction from surface contours for head CT examinations. *J Comput Assist Tomogr* 1981;5:60–7.
2. Batnitzky S, Price HI, Lee KR, et al. Three-dimensional computer reconstructions of brain lesions from surface contours provided by computed tomography: a prospectus. *Neurosurgery* 1982;11:73–84.
3. Armstrong EA, Smith TH, Currarino G. 3D CT reconstruction in children. Presented at the 69th Scientific Assembly and Annual Meeting of the Radiological Society of North America, Chicago, Nov. 13–18, 1983.
4. Vannier MW, Gado MH, Marsh JL. Three-dimensional display of intracranial soft-tissue structures. *AJNR* 1983;4: 520–1.
5. Herman GT, Vose WF, Gomori JM, Gefter WB. Stereoscopic computed three-dimensional surface displays. *RadioGraphics* 1985;5:825–52.
6. Altman NR, Altman DH, Wolfe SA, Morrison G. Three-dimensional CT reformation in children. *AJNR* 1986;7:287–93.
7. Gillespie JE, Isherwood I. Three-dimensional anatomical images from computed tomographic scans. *Br J Radiol* 1986;59:289–92.
8. Lobregt S, Kleine Schaars HWG. Three-dimensional imaging and manipulation of CT data. *Medicamundi* 1987;32: 92–8.
9. Cline HE, Lorensen WE, Ludke S, Crawford CR, Teeter BC. Two algorithms for the three-dimensional reconstruction of tomograms. *Med Phys* 1988;15:320–7.